Soft Matter

Oxidative instability of boronic acid-installed polycarbonate nanoparticles

Journal:	*Soft Matter*
Manuscript ID	SM-ART-12-2019-002499.R1
Article Type:	Paper
Date Submitted by the Author:	04-Feb-2020
Complete List of Authors:	Herrera-Alonso, Margarita; Colorado State University, Chemical and Biological Engineering Garcia, Elena; Colorado State University, Chemical and Biological Engineering Pessoa, Diogo; Tempus

ARTICLE

Oxidative instability of boronic acid-installed polycarbonate nanoparticles

Received 00th January 20xx,
Accepted 00th January 20xx

DOI: 10.1039/x0xx00000x

Elena A. Garcia,[a] Diogo Pessoa[b] and Margarita Herrera-Alonso[a]†

Oxidative stress, caused by the overproduction of reactive oxygen species (ROS), is often observed in degenerative and/or metabolic diseases, tumors, and inflamed tissues. Boronic acids are emerging as a unique class of responsive biomaterials targeting ROS because of their reactivity toward H_2O_2. Herein, we examine the oxidative reactivity of nanoparticles from a boronic acid-installed polycarbonate. The extent of oxidation under different concentrations of H_2O_2 was tracked by the change in fluorescence intensity of an encapsulated solvatochromic reporter dye, demonstrating their sensitivity to biologically-relevant concentrations of hydrogen peroxide. Oxidation-triggered particle destabilization, however, was shown to be highly dependent on the concentration of the final oxidized polymer product, and was only achieved if it fell below polymer critical micelle concentration. Our results indicate that these nanocarriers serve as an excellent dual pH/H_2O_2 responsive vehicle for drug delivery.

Introduction

Stimuli-responsive nanocarriers for the targeted delivery of therapeutics have recently attracted a great deal of attention in the field of nanomedicine.[1-3] One of the advantages of environmentally sensitive delivery vehicles is their ability to undergo physicochemical changes upon exposure to external signals and to subsequently release their payload at target sites.[4] Although a variety of nanocarriers can be fabricated from different materials such as lipids and metals[2], polymeric nanoparticles in particular have gained significant interest due to their chemical versatility. Recent advances in polymerization techniques have allowed the design and synthesis of polymers with well-defined chemistry and architecture that can be easily modified to render them responsive to a variety of physical[5-8] (e.g. light, temperature, ultrasound, magnetic field, electric field) or chemical[9-10] (e.g. enzymatic activity, ionic strength, redox potential, pH, oxidative conditions) external stimuli.[2-3] As often times observed in nature, many biological processes result from adjustment not to one, but several environmental changes.[3] Therefore, it is of great interest to design polymeric materials that are capable of responding to multiple stimuli. Some of the most commonly studied multi-responsive systems are formulated from macromolecules triggered by temperature/light,[11-12] temperature/pH,[13-16] pH/redox[17-20] and pH/salt.[21] Far less explored are dual-responsive systems that use temperature, redox potential or pH in combination with oxidation.

Reactive oxygen species (such as hydrogen peroxide, superoxide and hypochlorite) play a crucial role in a variety of physiological processes such as cell signaling and defense against infections.[22-23] However, oxidative stress, which is caused by the overproduction of ROS (particularly H_2O_2), is often observed in degenerative and/or metabolic diseases, tumorous and inflamed tissue, and is known to modulate cancer metastasis.[22-25] Not only is hydrogen peroxide concentration inside cancerous cells elevated to as high as 100 μM H_2O_2, but some cancer cells can tolerate extracellular H_2O_2 concentration up to 10 mM.[26]

Boronic acids and their derivatives are emerging as a unique class of responsive materials for biomedical applications. The growing appeal of boronic acids stems from their ability to form reversible boronic esters with 1,2- or 1,3-diols and catechol-containing molecules, as well as their pH sensitivity and reactivity toward H_2O_2.[27-33] Although the application of boronic acid-based oxidation-sensitive materials for the "smart" delivery of therapeutics is relatively new, this area of research is expanding at a rather fast pace partially due the ease of functionalization of boronate moieties as well as their commercial availability.[22, 24-25, 28, 34-38]

The most commonly used synthetic techniques[39] for the preparation of organoboron polymers include either direct free radical living polymerization of boronic ester-containing acrylate, acrylamide, or styrene monomers through RAFT[40-46] and ATRP[47-49] mechanisms, or post-modification[28, 50-52] of preformed polymers with boronic acid-bearing moieties. One

[a] Department of Chemical and Biological Engineering, School of Advanced Materials Discovery, Colorado State University, Fort Collins, Colorado 80523.
[b] Current address: Tempus, 600 W Chicago Ave, Chicago, Illinois 60654.
† To whom the correspondence should be addressed.

Electronic Supplementary Information (ESI) available: The experimental section includes protocols for polymer synthesis and characterization, as well as NMR data of monomer and polymer, GPC of polymers, and critical micelle concentration results. Data for polymer nanoparticles include fluorescence, dynamic light scattering, electron microscopy images and zeta-potential measurements. See DOI: 10.1039/x0xx00000x

drawback of polymers prepared by these methods is biodegradability. Therefore, for biomedical applications it would be most advantageous to utilize polymer backbones capable of undergoing complete degradation over time. In particular, aliphatic polycarbonates (PCs) serve as a great alternative due to their excellent biocompatibility, biodegradability, good mechanical properties, low toxicity and non-acidity of their degradation by-products.[53-55] Part of their appeal stems from the ease with which a great variety of functionalities can be appended to the PC backbone to render the polymer responsive to external stimuli.[56-58] Our group was the first to report on the synthesis of boronic acid-installed polymers by ring-opening polymerization,[59] and show their pH-triggered drug release capability in a nanoparticle form.[31] Since, other groups have developed alternative methods for their synthesis,[60-61] and studied their properties primarily in the context of biomedical applications.[24, 33, 62-65]

Herein, we examine the oxidative reactivity of nanoparticles from a boronic acid-installed polycarbonate. The extent of oxidation under different concentrations of H_2O_2 was tracked by the change in fluorescence intensity of an encapsulated solvatochromic reporter dye, showing that nanoparticles were sensitive to biologically-relevant concentrations of hydrogen peroxide and that the extent of oxidation directly reflects the amount of the oxidant present. Notably, oxidation-triggered particle destabilization was shown to be highly dependent on the concentration of the final oxidized polymer product, and was only achieved if it fell below the critical micelle concentration of the oxidized polymer. Our results indicate that these nanocarriers serve as an excellent dual pH/H_2O_2 responsive vehicle for drug delivery and highlight the importance of polymer concentration on particle destabilization.

Experimental

Details regarding materials synthesis and characterization are provided in the Supporting Information.

Results and Discussion

Monomer oxidation

To study the oxidation of boronic acid-installed polycarbonates in a nanoparticle form, we first examined monomer oxidation in either deuterium oxide or deuterated phosphate buffer (0.5x PBS) by ^{1}H NMR. Due to its poor solubility in polar solvents, monomer oxidation was examined in solutions of d_6-DMSO and D_2O. Oxidation experiments were carried out at 37 °C with different H_2O_2 concentrations.

The mechanism of oxidation of monomer **1** (**Figure 1**) follows that previously observed for the oxidation of a carbamate-linked phenylboronic acid derivative of trimethylene carbonate,[25] and for the H_2O_2-triggered oxidation of a phenylboronic acid-installed acrylate monomer.[23] As the NMR spectra show, monomer **1** and its hydrolyzed analog **2**, are oxidized to 4-hydroxybenzyl cyclic carbonate **3** and pinacol boric ester. The latter is further hydrolyzed to free pinacol and boric acid, which is evidenced by the gradual conversion of signal g' to g''. Since mildly basic conditions are required for the decomposition of 4-hydroxybenzyl cyclic carbonate,[23] when in PBS, compound **3** quickly breaks down to form 2-methyl-2-carboxyl-propylene carbonate **4** (MCC) and the highly reactive intermediate *p*-quinone methide **5**. The latter can then either react directly with H_2O to form 4-(hydroxymethyl)phenol **6**, or it can first react with HPO_4^{2-} (or $H_2PO_4^-$) to form 4-hydroxybenzyl phosphate **7**, which in turn is gradually hydrolyzed to **6**. The extent of monomer oxidation can be calculated with the relative amounts of **6** and **7**.

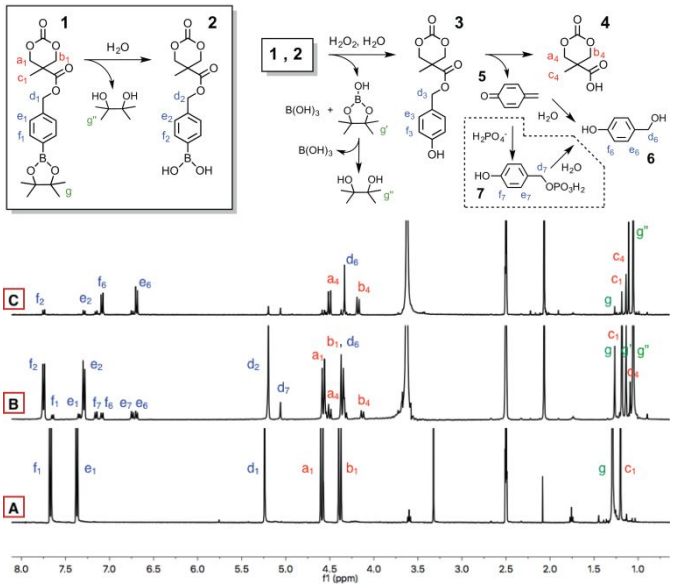

Figure 1. Top: Oxidation of monomer **1** in phosphate buffer and water (excluding the dotted region). Bottom: Oxidation of monomer **1** at 50 mM H_2O_2 in deuterated PBS/d_6-DMSO tracked by ^{1}H NMR. Spectrum A corresponds to monomer **1**; spectra B and C correspond to oxidation periods of 5 h and 6 days, respectively.

Monomer oxidation in water showed a slightly different behavior to that previously discussed for the buffered system. As expected in the absence of PBS, signals corresponding to 4-hydroxybenzyl phosphate **7** were not detected. Instead, peaks corresponding to 4-hydroxybenzyl cyclic carbonate **3** were directly observed. As oxidation proceeded, the pH of the system gradually drops because the acidic MCC product **4** cannot be neutralized. Since mildly basic conditions are required for complete decomposition of **3** into *p*-quinone methide **5**, the decrease in pH leads to eventual accumulation of the oxidation intermediate. The most notable difference between the oxidation behavior of **1** and **2** in buffered and non-buffered systems, is that as the pH drops below the pKa of the boronic ester in the non-buffered case, the complex is converted from its tetrahedral form to a much less hydrolytically stable trigonal neutral form, which leads to its dissociation. Since boronic esters are much more acidic than their parent free acids, the loss of the diol renders the boronic center less electrophilic. Considering that oxidation by hydrogen peroxide is a nucleophilic attack on boron, the

decrease in electrophilicity of the boron center, therefore, slows down the oxidation process.

Oxidation of unloaded nanoparticles

The oxidation kinetics of PEG_{45}-*b*-$PPBC_{26}$ (**P1**) nanoparticles (unloaded) was analyzed by ^1H NMR to < 30 h. Details regarding sample preparation (i.e., incubation, lyophilization and NMR acquisition) are provided in the Supporting Information and selected spectra are presented in **Figure 2**. The extent of polymer oxidation was calculated using the relative amounts of the methylene peak of 4-(hydroxymethyl)phenol (signal d_6) and **P3**, to the remaining species. A similar protocol was used to analyze copolymer oxidation in phosphate buffer, with the exception that nanoparticles were dialyzed against 0.1X PBS for 3.5 h prior to incubation studies.

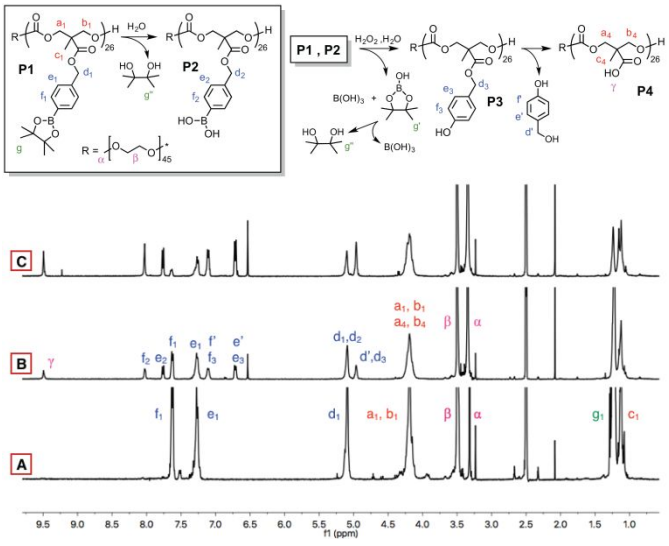

Figure 2. Top: oxidation of PEG_{45}-*b*-$PPBC_{26}$ (**P1**) nanoparticles in water. Bottom: oxidation of **P1** nanoparticles at 500 µM H_2O_2 tracked by ^1H NMR. Spectrum A corresponds to polymer **P1**; spectra B, C and D correspond to oxidation periods of 2.5 h and 20 h respectively.

Oxidation of un-loaded polymer nanoparticles was initially examined with a hydrogen peroxide concentration of 500 µM, which in this case corresponds to a H_2O_2:B molar ratio of 0.56. Samples analyzed after nanoparticle preparation, and in the absence of hydrogen peroxide, showed limited oxidation (~ 6%), which we attributed to the presence of peroxides in the solvent (THF) that was used to dissolve the polymer for self-assembly. Subsequent experiments were carried out using THF stabilized with BHT to preclude this "unwanted" reaction. Regardless of oxidation time, NMR spectra showed no evidence of backbone degradation under the examined conditions which is consistent with the fact that alkaline environments are required for carbonate hydrolysis.[55]

Oxidation in both H_2O and 0.1X PBS exhibited a similar trend: ~30% of polymer oxidized after 7 h of incubation reaching a plateau at 50% within 30 h (**Figure S6**). This result shows that all of the hydrogen peroxide in the system was consumed and further demonstrates that it is possible to control the extent of polymer oxidation by varying the molar equivalents of H_2O_2 to boronic acid. If the goal at hand is to design a system where a payload is released from the nanoparticle core upon encountering an oxidative environment, we predict that micelles prepared from PEG_{45}-*b*-$PPBC_{26}$ copolymer can be an excellent candidate as oxidation-sensitive delivery vehicles.

Oxidation of nile red encapsulated PEG_{45}-b-$PPBC_{26}$ nanoparticles

Nile red (NR) nanoparticles stabilized by **P1 (**PEG_{45}-*b*-$PPBC_{26}$**)** were prepared by flash nanoprecipitation as described in the Supporting Information. The final polymer concentration after dialysis was ~ 0.41% w_p/w and the concentration of nile red was 0.1% w/w_p. Nanoparticle size and polydispersity, after dialysis to remove the organic solvent, were 39 nm and 0.11, respectively (**Figure S7**). TEM also showed well-defined particles with no aggregation. To track the decrease in fluorescence intensity, NR emission was measured from 550 to 800 nm with an excitation wavelength of λ_{ex} = 550 nm. Nanoparticle oxidation in 1X PBS was examined for three hydrogen peroxide concentrations (0, 250 and 1000 µM H_2O_2) and up to 24 h (**Figure 3**). While most of these concentrations are higher than the physiologically relevant range (50-100 µM),[22, 24, 66] for the particular experimental conditions examined they correspond to H_2O_2:B molar ratios of 0, 0.28 and 1.16. The effect of hydrogen peroxide concentration on the fluorescence of Nile Red is also included in the Supporting information (**Figure S8**). As shown, there is no observable effect of H_2O_2 concentration on NR fluorescence, aside from the shift in peak position which results from a change in the polarity of the solvent (see comparison with water).

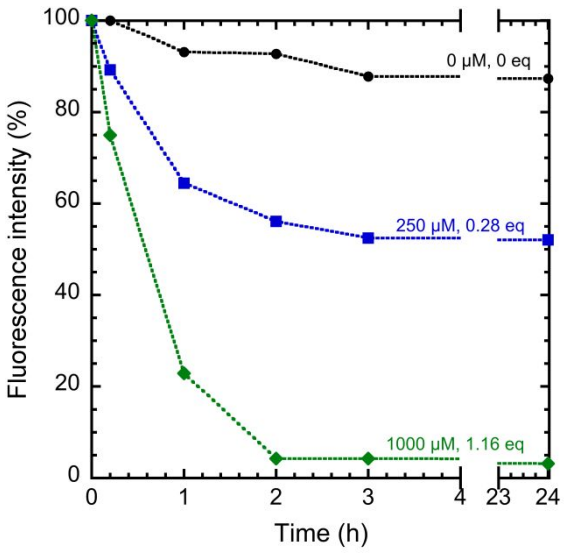

Figure 3. Fluorescence of nile red-loaded **P1** nanoparticles in PBS. Also shown are the corresponding H_2O_2:B molar ratios for each sample.

As shown in **Figure 3**, a clear decrease in NR fluorescence intensity was observed over time, the extent of which

depended on the H_2O_2:B molar ratio. Regardless of H_2O_2 concentration, the decay in fluorescence plateaus at ~ 3 h, with insignificant changes up to 24 h. As also shown in Figure **3**, the fluorescence intensity of the sample incubated in PBS in the absence of hydrogen peroxide decreased by ~ 12% in 3 h, which we attribute to hydrolysis of the boronic ester moiety resulting in an increase of the hydrophilic character of the core. The increase of core hydrophilicity is further confirmed by the slight red-shift in the fluorescence emission maximum of NR (**Figure S9**).

The sample containing 250 µM H_2O_2 shows a final fluorescence intensity of 52% which is lower than the predicted value of 72% based on the H_2O_2:B molar ratio used. The difference between experimental and theoretical values is attributed to hydrolysis. As oxidation proceeds, **P1** (PEG_{45}-*b*-$PPBC_{26}$, **Figure 2**) and its hydrolyzed analog **P2**, are gradually converted into **P3** and ultimately **P4** (PEG_{45}-*b*-PCC_{26}). As oxidation proceeds, the hydrophilic character of the core is expected to increase, particularly so when contrasting **P1** and **P4**; this difference is less pronounced when comparing **P2** and **P4**. Nevertheless, increased core hydrophilicity caused by pendant carboxylates resulting from oxidation could facilitate the influx of water and thus enable hydrolysis to proceed to a greater extent than observed for the sample free of hydrogen peroxide.

Zeta potential measurements were also used to assess nanoparticle oxidation in PBS. The zeta potential of nanoparticles in PBS was initially (prior to oxidation) -34 mV. Since the pKa of the phenylboronic acid pinacol ester is expected to be 2-4 units lower than the pKa of its deprotected acid form (pKa ~ 9.3),[27] it is possible that at pH 7.4, the phenyl boronic ester can act as a Lewis acid and coordinate an OH group to form a tetrahedral anionic species yielding a initial negative zeta potential. Upon oxidation, zeta potentials drop to ~ -70 mV and are seemingly insensitive to H_2O_2 concentration (**Figure S10**). This result is consistent with the presence of exposed carboxylic acids, resulting from polymer oxidation.

Oxidation of nanoparticles in Milli-Q water (pH ~ 6) was also examined (**Figure 4**). Similar to PBS, a decrease in NR fluorescence intensity with H_2O_2 concentration was observed over time and attributed to a combination of hydrolysis and oxidation. In this case, the decrease in fluorescence intensity assigned purely to hydrolysis reached 25% over a 30 h period. We had previously observed a similar pH-dependent trend for the release of capecitabine from PEG-*b*-PPBC nanoparticles.[31] Comparing **Figures 3** and **4**, it is clear that the combined rates of hydrolysis and oxidation are considerably slower in water than in PBS for the same H_2O_2 concentration. Furthermore, the difference of fluorescence intensity between samples containing H_2O_2 and those free of the the oxidant are greater for reactions in PBS. These differences are attributed to both the higher electrophilicity of the boronic ester compared to its deprotected parent acid,[67] as well as the increased rate of decomposition of the phenolic intermediate under mildly basic conditions.

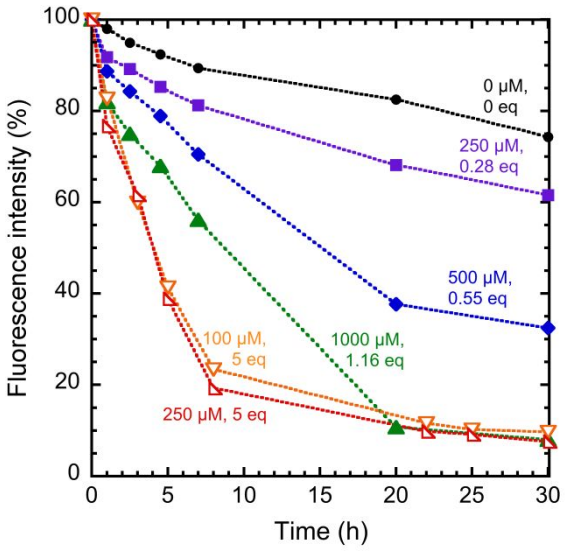

Figure 4. Fluorescence of nile red-loaded **P1** nanoparticles in water at 37 °C and different H_2O_2 concentrations. Also shown are the corresponding H_2O_2:B ratios for each sample. Closed and open symbols correspond to samples where the final polymer concentration was higher or lower than the C_{CMC} of the fully oxidized copolymer, respectively.

Although hydrolysis and/or oxidation increase the polarity inside nanoparticle cores resulting in the quenching of nile red fluorescence, this decrease does not necessarily imply nile red release from the core as a result of nanoparticle degradation. To examine this, dynamic light scattering measurements were taken throughout the oxidation process to interrogate for changes in particle size and dispersity. Size distributions of nanoparticles oxidized in water at different concentrations and times are provided in **Figure 5**. Interestingly, the sample run at 1000 µM (H_2O_2:B = 1.16, **A** in **Figure 5**) showed little to no change in particle size but a slight broadening of the distribution at long reaction times. This result is unexpected as the polarity inside the core is considerably enhanced upon oxidation. Prior examples of oxidation-triggered nanocarrier disassembly have shown to be induced by the change in polymer solubility due to cleavage of hydrophobic pendant groups[24, 28, 37, 68-69] or complete degradation of the polymer backbone.[25, 35, 38, 70] Fu, *et al.*,[24] for example, studied the fluorescence behavior of a series of triblock copolymers consisting of polycarbonate backbones with side-chains of diethylene glycol and either boronic acid-containing aliphatic or aromatic moieties. They showed that phenylboronic acid-containing polymers, in contrast to their aliphatic counterparts, underwent disassembly upon oxidation. A few important considerations must be made at this point to explain our results in light of Fu's work. Firstly, polymer architecture is known to have a highly consequential effect on the properties of their self-assemblies. Diblock and triblock copolymers with similar hydrophobic/hydrophilic compositions have, for example, different critical micelle concentrations, generally lower for diblocks, as well as different intermicellar exchange rates, considerably faster for the triblock.[71-76] Explaining our differences in terms of the thermodynamic

stability of the assemblies based on the structure of the building blocks is not direct, as there exist important differences in terms of monomer arrangement (triblock vs. diblock), hydrophilic block chemistry, hydrophobic block length (which differs by a factor of 2), and hydrophilic contribution (i.e., number of ethylene glycol repeats which differ by a factor of 6). Second, though not explicitly mentioned by the Authors, we estimated that the H_2O_2:B ratio used by Fu was several orders of magnitude higher than the maximum used in our case, roughly 445 times higher than the nearly-stoichiometric ratio used by us. Lastly, the presence of unimers was observed by Fu et al. after 48 h of exposure to H_2O_2 under these conditions; our experiments were limited to < 30 h. Combined, these results help to explain the different behavior observed in both cases.

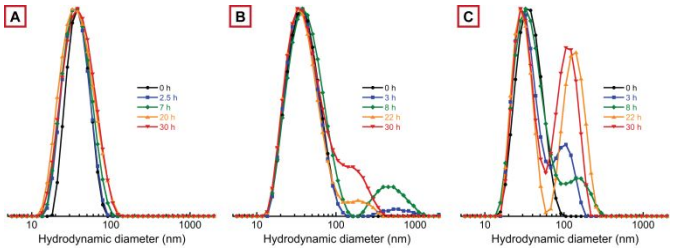

Figure 5. Size distributions of nile red encapsulated **P1** nanoparticles incubated at 37 °C in water. (A) Nanoparticles oxidized in 1000 μM H_2O_2 with a H_2O_2:B ratio of 1.16. (B) Nanoparticles oxidized in 250 μM H_2O_2 with a H_2O_2:B ratio of 5. (C) Nanoparticles oxidized in 100 μM H_2O_2 with a H_2O_2:B ratio of 5.

To further probe conditions leading to disassembly, we examined the effect of polymer concentration. For this, we first measured the critical micelle concentration of the fully oxidized copolymer **P4** ($C_{CMC,P4}$ = 68.5 μg/mL, **Figure S4**), and found it to be substantially higher than either that of the precursor polymer **P1** ($C_{CMC,P1}$ = 1.45 μg/mL) or of the hydrolyzed copolymer **P2** ($C_{CMC,P2}$ = 3.65 μg/mL). A roughly similar increase in critical micelle concentration had been reported for benzyl-protected vs. deprotected PEG-*b*-PCC.[54] While it is true that the polarity of the polycarbonate block changes upon oxidation, the hydrophobic character of the backbone continues to contribute to the overall water-solubility of this block. Despite the significant change in C_{CMC} of **P4**, the final polymer concentration of sample **A** in **Figure 5** exceeded the C_{CMC} of the fully oxidized copolymer therefore contributing to NP stability.

Oxidation was, therefore examined for samples whose supersaturation decreased below their C_{CMC} upon complete reaction. Supersaturation (S) is defined as the ratio of the polymer concentration to its critical micelle concentration. The concentration of H_2O_2 in these samples was 100 μM and 250 μM, such that the H_2O_2:B molar ratio in both cases was 5, exceeding the H_2O_2:B ratio previously discussed. For the 100 μM sample, $S_{initial(P1)}$=6.2 and $S_{final(P4)}$=0.055, whereas for the 250 μM case, $S_{initial(P1)}$=15.4 and $S_{final(P4)}$=0.138. As a reference, supersaturations for the previously discussed 1000 μM sample were $S_{initial(P1)}$ = 266 and $S_{final(P4)}$ = 2.4. As shown in **Figure 4** (open symbols), a considerably faster decay in fluorescence intensity was observed for samples oxidized in the presence of a 5-fold excess H_2O_2, with little difference between the 100 μM and 250 μM samples. At long reaction times, the fluorescence intensity of all samples at or above the stoichiometric ratio of H_2O_2:B plateau at the lowest attainable value (~7.5%).

Dynamic light scattering experiments of dilute nanoparticles revealed broadening distributions as oxidation proceeded, indicating either particle swelling or agglomeration. A more pronounced effect was noted for the sample with lower supersaturation values (**C** in **Figure 5**), wherein observable destabilization was evident even at short reaction times (3 h). Samples oxidized at higher polymer concentration (i.e., below the stoichiometric ratio of H_2O_2:B), showed little to no variation in particle size over 32 h.

Scattered light intensity measurements from DLS also provide useful information regarding nanoparticle concentration and number. The derived photon count rate, given as kilo counts per second (kCPS), can be used to monitor the kinetics of nanoparticle disassembly.[77-81] As shown in **Figure 6**, the derived count rate decreased during oxidation, with a faster decay for the sample with lowest supersaturation. In contrast, the sample incubated in the absence of H_2O_2 showed no considerable variation over time. The decay in derived photon count rate is indicative of a reduction in particle number and/or size.[82] As the electrostatic repulsion of negatively charged carboxylate groups, resulting from oxidation, would contribute to core swelling, the decay can only be explained by a decrease in the number of particles thus confirming that oxidation leads to destabilization and disassembly under the conditions examined.

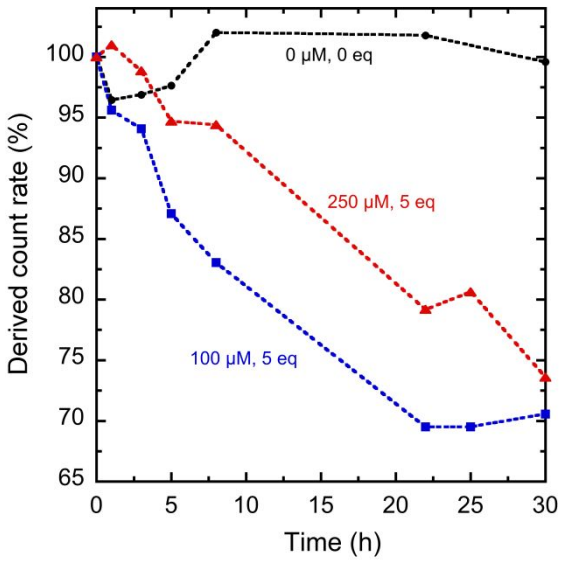

Figure 6. Derived count rate of nile red-loaded **P1** nanoparticles in water at 37 °C and different H_2O_2 concentrations.

Conclusions

We have systematically studied the oxidation of nanoparticles formed from diblock copolymers containing a phenylboronic acid-functionalized polycarbonate (PPBC) in the presence of hydrogen peroxide at physiologically-relevant concentrations. Our results show that the extent and rate of oxidation are not only directly dependent on the ratio of hydrogen peroxide to boron, but also appear to be faster in buffered environments. However, and despite the change in core polarity due to oxidation, particle destabilization was strongly dependent on polymer concentration and was only achieved if the final concentration fell below the critical micelle concentration of the oxidized polymer. When designing a system for cargo release in an oxidative environment, it is important to keep in mind the mechanism by which this payload should be delivered. If the goal is to release the payload complexed to the polymer backbone, it can be readily accomplished by exposing nanoparticles to an oxidative environment; in this case, the amount of bound cargo detached will be directly related to the concentration of the oxidant. If particle destabilization and disassembly is desired, polymer concentration relative to the critical micelle concentration of the end product will play a critical role. A variety of drugs or imaging agents bearing a 1,2-diol can be readily complexed to phenylboronic acid-containing polymers resulting in polymer-drug conjugates which are reactive toward physiologically-relevant changes in pH and, as we show here, H_2O_2 levels.

Conflicts of interest

There are no conflicts to declare.

Acknowledgements

We acknowledge financial support by the National Science Foundation (CMMI-1562639).

Notes and references

1 M. A. C. Stuart, W. T. S. Huck, J. Genzer, M. Muller, C. Ober, M. Stamm, G. B. Sukhorukov, I. Szleifer, V. V. Tsukruk, M. Urban, F. Winnik, S. Zauscher, I. Luzinov and S. Minko, *Nature Materials*, 2010, **9**, 101-113.
2 M. Elsabahy and K. L. Wooley, *Chem Soc Rev*, 2012, **41**, 2545-2561.
3 J. M. Zhuang, M. R. Gordon, J. Ventura, L. Y. Li and S. Thayumanavan, *Chemical Society Reviews*, 2013, **42**, 7421-7435.
4 W. W. Gao, J. M. Chan and O. C. Farokhzad, *Mol Pharmaceut*, 2010, **7**, 1913-1920.
5 H. G. Schild, *Prog Polym Sci*, 1992, **17**, 163-249.
6 J. Xu, S. Z. Luo, W. F. Shi and S. Y. Liu, *Langmuir*, 2006, **22**, 989-997.
7 Y. J. Zhang and P. S. Cremer, *Curr Opin Chem Biol*, 2006, **10**, 658-663.
8 S. Z. Luo, C. X. Ling, X. L. Hu, X. Liu, S. S. Chen, M. C. Han and J. A. Xia, *J Colloid Interf Sci*, 2011, **353**, 76-82.
9 J. H. Ryu, R. T. Chacko, S. Jiwpanich, S. Bickerton, R. P. Babu and S. Thayumanavan, *Journal of the American Chemical Society*, 2010, **132**, 17227-17235.
10 J. H. Ryu, S. Bickerton, J. M. Zhuang and S. Thayumanavan, *Biomacromolecules*, 2012, **13**, 1515-1522.
11 T. Shimoboji, E. Larenas, T. Fowler, S. Kulkarni, A. S. Hoffman and P. S. Stayton, *P Natl Acad Sci USA*, 2002, **99**, 16592-16596.
12 F. D. Jochum and P. Theato, *Chemical Society Reviews*, 2013, **42**, 7468-7483.
13 C. Pietsch, R. Hoogenboom and U. S. Schubert, *Angew Chem Int Edit*, 2009, **48**, 5653-5656.
14 M. Gao, X. R. Jia, Y. Li, D. H. Liang and Y. Wei, *Macromolecules*, 2010, **43**, 4314-4323.
15 T. Ta, A. J. Convertine, C. R. Reyes, P. S. Stayton and T. M. Porter, *Biomacromolecules*, 2010, **11**, 1915-1920.
16 W. Cui, X. M. Lu, K. Cui, L. Niu, Y. Wei and Q. H. Lu, *Langmuir*, 2012, **28**, 9413-9420.
17 J. Chen, X. Z. Qiu, J. Ouyang, J. M. Kong, W. Zhong and M. M. Q. Xing, *Biomacromolecules*, 2011, **12**, 3601-3611.
18 C. Wei, J. Guo and C. Wang, *Macromol Rapid Commun*, 2011, **32**, 451-455.
19 A. W. Jackson and D. A. Fulton, *Macromolecules*, 2012, **45**, 2699-2708.
20 X. L. Hu, H. Li, S. Z. Luo, T. Liu, Y. Y. Jiang and S. Y. Liu, *Polymer Chemistry*, 2013, **4**, 695-706.
21 Y. Kakizawa and K. Kataoka, *Adv Drug Deliver Rev*, 2002, **54**, 203-222.
22 C. de Gracia Lux, S. Joshi-Barr, T. Nguyen, E. Mahmoud, E. Schopf, N. Fomina and A. Almutairi, *J Am Chem Soc*, 2012, **134**, 15758-15764.
23 C. C. Song, R. Ji, F. S. Du, D. H. Liang and Z. C. Li, *Acs Macro Letters*, 2013, **2**, 273-277.
24 Y. H. Fu, C. Y. Chen and C. T. Chen, *Polymer Chemistry*, 2015, **6**, 8132-8143.
25 F. Y. Qiu, C. C. Song, M. Zhang, F. S. Du and Z. C. Li, *Acs Macro Lett*, 2015, **4**, 1220-1224.
26 H. Hagen, P. Marzenell, E. Jentzsch, F. Wenz, M. R. Veldwijk and A. Mokhir, *Journal of Medicinal Chemistry*, 2012, **55**, 924-934.
27 G. Springsteen and B. H. Wang, *Tetrahedron*, 2002, **58**, 5291-5300.
28 K. E. Broaders, S. Grandhe and J. M. J. Frechet, *Journal of the American Chemical Society*, 2011, **133**, 756-758.
29 J. N. Cambre and B. S. Sumerlin, *Polymer*, 2011, **52**, 4631-4643.
30 J. Su, F. Chen, V. L. Cryns and P. B. Messersmith, *Journal of the American Chemical Society*, 2011, **133**, 11850-11853.
31 Y. E. Aguirre-Chagala, J. L. Santos, Y. X. Huang and M. Herrera-Alonso, *Acs Macro Letters*, 2014, **3**, 1249-1253.
32 F. Coumes, P. Woisel and D. Fournier, *Macromolecules*, 2016, **49**, 8925-8932.
33 G. Vancoillie and R. Hoogenboom, *Polym Chem-Uk*, 2016, **7**, 5484-5495.
34 C. Y. Chen and C. T. Chen, *Chemistry*, 2013, **19**, 16050-16057.
35 C. C. Song, R. Ji, F. S. Du and Z. C. Li, *Macromolecules*, 2013, **46**, 8416-8425.
36 F. Y. Qiu, M. Zhang, R. Ji, F. S. Du and Z. C. Li, *Macromol Rapid Commun*, 2015, **36**, 2012-2018.
37 E. Jager, A. Hocherl, O. Janouskova, A. Jager, M. Hruby, R. Konefal, M. Netopilik, J. Panek, M. Slouf, K. Ulbrich and P. Stepanek, *Nanoscale*, 2016, **8**, 6958-6963.
38 A. Iturmendi, U. Monkowius and I. Teasdale, *Acs Macro Letters*, 2017, **6**, 150-154.
39 W. L. A. Brooks and B. S. Sumerlin, *Chemical Reviews*, 2016, **116**, 1375-1397.
40 J. N. Cambre, D. Roy, S. R. Gondi and B. S. Sumerlin, *J Am Chem Soc*, 2007, **129**, 10348-10349.

41 D. Roy, J. N. Cambre and B. S. Sumerlin, *Chem Commun (Camb)*, 2008, DOI: 10.1039/b802293c, 2477-2479.
42 P. De, S. R. Gondi, D. Roy and B. S. Sumerlin, *Macromolecules*, 2009, **42**, 5614-5621.
43 K. T. Kim, J. J. L. M. Cornelissen, R. J. M. Nolte and J. C. M. van Hest, *Journal of the American Chemical Society*, 2009, **131**, 13908-+.
44 A. P. Bapat, D. Roy, J. G. Ray, D. A. Savin and B. S. Sumerlin, *Journal of the American Chemical Society*, 2011, **133**, 19832-19838.
45 H. Kim, Y. J. Kang, S. Kang and K. T. Kim, *Journal of the American Chemical Society*, 2012, **134**, 4030-4033.
46 S. Maji, G. Vancoillie, L. Voorhaar, Q. L. Zhang and R. Hoogenboom, *Macromolecular Rapid Communications*, 2014, **35**, 214-220.
47 Y. Qin, V. Sukul, D. Pagakos, C. Z. Cui and F. Jakle, *Macromolecules*, 2005, **38**, 8987-8990.
48 K. T. Kim, J. J. L. M. Cornelissen, R. J. M. Nolte and J. C. M. van Hest, *Advanced Materials*, 2009, **21**, 2787-+.
49 Y. Yao, X. M. Wang, T. W. Tan and J. Yang, *Soft Matter*, 2011, **7**, 7948-7951.
50 C. Z. Cui, E. M. Bonder, Y. Qin and F. Jakle, *J Polym Sci Pol Chem*, 2010, **48**, 2438-2445.
51 R. J. Ma, H. Yang, Z. Li, G. Liu, X. C. Sun, X. J. Liu, Y. L. An and L. Q. Shi, *Biomacromolecules*, 2012, **13**, 3409-3417.
52 E. Montanari, A. Gennari, M. Pelliccia, C. Gourmel, E. Lallana, P. Matricardi, A. J. McBain and N. Tirelli, *Macromol Biosci*, 2016, **16**, 1815-1823.
53 H. L. Guan, Z. G. Xie, P. B. Zhang, X. Wang, X. S. Chen, X. H. Wang and X. B. Jing, *J Polym Sci Pol Chem*, 2005, **43**, 4771-4780.
54 F. Li, M. Danquah and R. I. Mahato, *Biomacromolecules*, 2010, **11**, 2610-2620.
55 F. Suriano, O. Coulembier, J. L. Hedrick and P. Dubois, *Polymer Chemistry*, 2011, **2**, 528-533.
56 R. C. Pratt, F. Nederberg, R. M. Waymouth and J. L. Hedrick, *Chemical Communications*, 2008, DOI: 10.1039/b713925j, 114-116.
57 S. Tempelaar, L. Mespouille, P. Dubois and A. P. Dove, *Macromolecules*, 2011, **44**, 2084-2091.
58 S. Tempelaar, I. A. Barker, V. X. Truong, D. J. Hall, L. Mespouille, P. Dubois and A. P. Dove, *Polymer Chemistry*, 2013, **4**, 174-183.
59 Y. E. Aguirre-Chagala, J. L. Santos, B. A. Aguilar-Castillo and M. Herrera-Alonso, *Acs Macro Letters*, 2014, **3**, 353-358.
60 R. J. Ono, S. Q. Liu, S. Venkataraman, W. L. Chin, Y. Y. Yang and J. L. Hedrick, *Macromolecules*, 2014, **47**, 7725-7731.
61 N. H. Park, Z. X. Voo, Y. Y. Yang and J. L. Hedrick, *Acs Macro Lett*, 2017, **6**, 252-256.
62 Y. Dai and X. J. Zhang, *Polym Chem-Uk*, 2017, **8**, 7429-7437.
63 S. Obuobi, Z. X. Voo, M. W. Low, B. Czarny, V. Selvarajan, N. L. Ibrahim, Y. Y. Yang and P. L. R. Ee, *Adv Healthc Mater*, 2018, **7**.
64 T. Kubo, G. M. Scheutz, T. S. Latty and B. S. Sumerlin, *Chem Commun*, 2019, **55**, 5655-5658.
65 J. P. K. Tan, Z. X. Voo, S. Lim, S. Venkataraman, K. M. Ng, S. J. Gao, J. L. Hedrick and Y. Y. Yang, *Nanomed-Nanotechnol*, 2019, **17**, 236-245.
66 B. Halliwell, M. V. Clement and L. H. Long, *Febs Lett*, 2000, **486**, 10-13.
67 X. L. Sun, S. Y. Xu, S. E. Flower, J. S. Fossey, X. H. Qian and T. D. James, *Chemical Communications*, 2013, **49**, 8311-8313.
68 C. Y. Chen and C. T. Chen, *Chem-Eur J*, 2013, **19**, 16050-16057.
69 F. Y. Qiu, M. Zhang, R. Ji, F. S. Du and Z. C. Li, *Macromol Rapid Comm*, 2015, **36**, 2012-2018.
70 C. D. Lux, S. Joshi-Barr, T. Nguyen, E. Mahmoud, E. Schopf, N. Fomina and A. Almutairi, *J Am Chem Soc*, 2012, **134**, 15758-15764.
71 P. Alexandridis, V. Athanassiou, S. Fukuda and T. A. Hatton, *Langmuir*, 1994, **10**, 2604-2612.
72 S. Creutz, J. vanStam, S. Antoun, F. C. DeSchryver and R. Jerome, *Macromolecules*, 1997, **30**, 4078-4083.
73 S. Dai, P. Ravi, C. Y. Leong, K. C. Tam and L. H. Gan, *Langmuir*, 2004, **20**, 1597-1604.
74 M. M. Mok, R. Thiagarajan, M. Flores, D. C. Morse and T. P. Lodge, *Macromolecules*, 2012, **45**, 4818-4829.
75 J. Lu, F. S. Bates and T. P. Lodge, *Macromolecules*, 2015, **48**, 2667-2676.
76 T. Zinn, L. Willner, V. Pipich, D. Richter and R. Lund, *Acs Macro Lett*, 2016, **5**, 884-888.
77 C. Sanson, C. Schatz, J. F. Le Meins, A. Brulet, A. Soum and S. Lecommandoux, *Langmuir*, 2010, **26**, 2751-2760.
78 Q. M. Liu, J. Chen and J. Z. Du, *Biomacromolecules*, 2014, **15**, 3072-3082.
79 T. Yildirim, A. Traeger, E. Preussger, S. Stumpf, C. Fritzsche, S. Hoeppener, S. Schubert and U. S. Schubert, *Macromolecules*, 2016, **49**, 3856-3868.
80 C. P. Jesson, V. J. Cunningham, M. J. Smallridge and S. P. Armes, *Macromolecules*, 2018, **51**, 3221-3232.
81 S. Van Herck, K. Deswarte, L. Nuhn, Z. Zhong, J. P. P. Catani, Y. Li, N. N. Sanders, S. Lienenklaus, S. De Koker, B. N. Lambrecht, S. A. David and B. G. De Geest, *J Am Chem Soc*, 2018, **140**, 14300-14307.
82 J. Shang and X. H. Gao, *Chem Soc Rev*, 2014, **43**, 7267-7278.

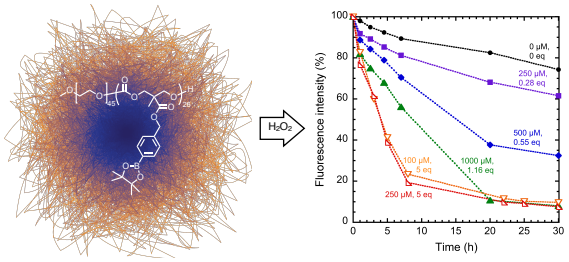
H_2O_2
Fluorescence intensity (%)
Time (h)
0 μM, 0 eq
250 μM, 0.28 eq
500 μM, 0.55 eq
1000 μM, 1.16 eq
100 μM, 5 eq
250 μM, 5 eq